Hysteresis and multistability at the transition to turbulence probed with a NEMS wire in superfluid helium

Š. Midlik[1], P. Danylchenko[1], A. N. Gheorghe[1], S. Harašta[1], J. Mikeš[1], D. E. Zmeev[2], D. Schmoranzer[1*†]

[1*]Faculty of Mathematics and Physics, Charles University, Ke Karlovu 3, Prague, 121 16, Czech Republic.
[2]Department of Physics, Lancaster University, Lancaster, LA1 4YB, United Kingdom.

*Corresponding author(s). E-mail(s): david.schmoranzer@matfyz.cuni.cz;
†All authors contributed equally to this work.

Abstract

We present experimental data on the transition to turbulent drag as measured with a superconducting nanowire resonator submerged in superfluid ^{4}He above 1 K. The transition shows clear hysteretic behaviour in switching between laminar and turbulent regimes, stronger than most previous works in the two-fluid regime. We present and discuss the temperature-dependence of this effect in connection to the instability of the flow in the superfluid component of He II. Additionally, multistability of the turbulent flow is reported, with three distinct metastable states appearing at temperatures below 1.5 K.

Keywords: superfluid helium, NEMS resonator, quantum turbulence, hysteresis, multistability

1 Introduction

The stability of laminar flow and the eventual transition to turbulence is one of the fundamental problems in fluid dynamics with numerous practical implications. In classical fluid dynamics, many known flow instabilities have been investigated, usually

specific to a given flow geometry, and a comprehensive body of literature exists on this topic [1, 2]. As a result, classical stability theory has acquired significant predictive capabilities, and the remaining open questions are mainly linked to the microscopic origins of the trigger events. In the context of nanowire resonators, the flow around an oscillating cylinder is of particular interest [3–7].

In quantum fluids such as superfluid helium, the same problem has been encountered as well. Few conclusive and comprehensive works exist, but numerous experiments have been already performed with various oscillators such as grids [8, 9], wires [10–13], spheres [14, 15], discs [16], tuning forks [17–20], or more recently nanofluidic Helmholtz resonators [21–23] and wire-like NEMS devices [24–26]. In this paper, we investigate the details of the transition to turbulence observed with a nanomechanical resonator – a superconducting NbTi wire of sub-micron thickness submerged in superfluid helium and driven using the magnetomotive scheme. In superfluid ^{4}He, the two-fluid model [27, 28] is used to describe the dynamics at temperatures above roughly 1 K. The model defines a normal viscous component of density ρ_n and an inviscid superfluid component of density ρ_s, with the total density $\rho = \rho_n + \rho_s$. In the superfluid component, quantized vortices exist [29, 30], each carrying one quantum of circulation, $\kappa = h/m_4 = 9.97 \times 10^{-8}$ m^{2}s^{-1}, where h is Planck's constant and m_4 is the mass of a ^{4}He atom. Therefore, in certain scenarios, the onset of turbulent flow is expected to be influenced by the quantized nature of circulation in the superfluid component and related to the mechanisms of quantized vortex nucleation and proliferation.

Past experiments with oscillators have shown the possibility of hysteretic behaviour at the transition to turbulence, with a bi-stable region of laminar and turbulent flow [8, 11, 19]. In this region, the flow was strongly history-dependent and could switch between the two regimes at random if left undisturbed for a sufficiently long time. If the size of the oscillator is small enough that a classical instability in the normal component is unlikely at the observed critical velocity, one may use this experiment to investigate the properties of individual quantized vortices and their role in the nucleation of quantum turbulence.

To rule out the classical instability, one needs to ensure that the relevant dimensionless parameter is below its critical value and that it does not govern the observed instability. In classical fluids, the parameter of choice is usually the oscillatory Reynolds number $\mathrm{Re}_\delta = U\delta/\nu$, where U is a characteristic velocity, $\delta = \sqrt{2\nu/\omega}$ is the viscous penetration depth (Stokes' boundary layer thickness), ν represents the kinematic viscosity and ω is the angular frequency of oscillation. For oscillators of size $D \gg \delta$, this is the only dynamically relevant parameter, while in other cases, the Stokes number $\beta = D^2/(\pi\delta^2)$ must also be considered [31]. In the context of superfluids, a parameter equivalent to Re_δ should be defined only for the normal component, replacing ν by η/ρ_n, and is usually called the Donnelly number [31–33]:

$$\mathrm{Dn} = U\rho_n\delta_n/\eta\,, \quad \delta_n = \sqrt{2\eta/(\rho_n\omega)}. \tag{1}$$

However, the above is applicable only if $D \gg \delta_n$. For the ratio of $D/\delta_n \approx 1$, an extension of the above theory may be formulated by computing the exact drag forces

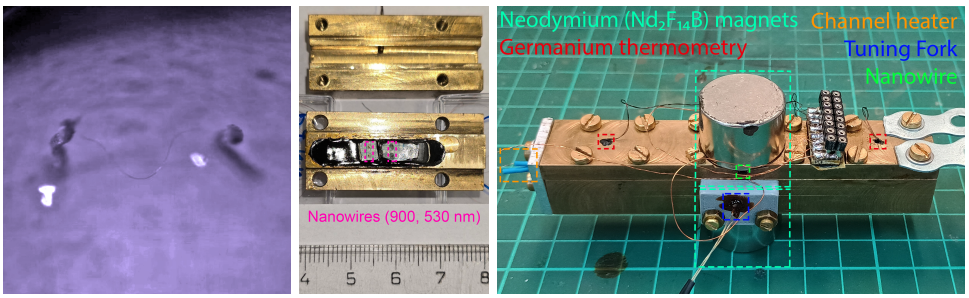

Fig. 1 Left: Optical micrograph of the 900 nm wire in blue light The device is suspended loosely between the remaining pieces of multifilament wire. Center: Short channel, open, with two devices (530 nm and 900 nm) in the center. Right: Long channel, closed, with 560 nm device installed and the two NdFeB magnets.

acting on the oscillator. For an oscillating cylinder, the relevant dynamical equations (neglecting the non-linear term) were written down already by Stokes [34] and their solution is today conveniently expressed [35] in terms of modified (cylindrical) Bessel functions or order n, K_n. It can be shown that compared to the drag in the high frequency limit, $F_{\rm hf}$, (i.e., for $D \gg \delta_n$), the true dissipative drag force, $F_{\rm full}$, increases by a factor γ, given by:

$$\gamma \equiv \frac{F_{\rm full}}{F_{\rm hf}} = \Re\left\{(1+i)\frac{K_0\left[(1+i)R/\delta\right]}{K_1\left[(1+i)R/\delta\right]}\right\} \tag{2}$$

As the oscillatory Reynolds number (or Donnelly number) represents the ratio of viscous forces to inertial forces, the extended Donnelly number has to be redefined as:

$$\mathrm{Dn}^* \equiv \gamma\,\mathrm{Dn}, \tag{3}$$

to account for the true magnitude of the viscous drag when $D \simeq \delta_n$. With this approach, the scaling laws previously derived for the high frequency limit [31] may still be applied to the flow with the aim of qualitatively characterising the instability. We note, however, that approximations were made in the solution to Stokes' oscillating cylinder problem. A more refined solution was obtained by Wang [36], who was able to incorporate finite order corrections for the non-linear effects occurring in the boundary layer in the limit of high frequencies. For example, his solution does not neglect the dc component of Reynolds stresses and thus also describes, to a finite precision, the flow field and drag resulting from acoustic streaming.

2 Experimental setup

The NbTi oscillator was prepared from a multifilament commercial superconducting wire (NbTi in Cu matrix) using a diamond die set to reduce the diameter of the entire wire (bringing the individual filaments below 1 μm). Then a piece of the wire was formed into a loop and glued to paper impregnated with Stycast 1266, followed by etching the loop in an aqueous solution of HNO_3 to liberate the filaments. To stop the etching, the solution was diluted and effectively replaced with distilled water. While

still in the diluted solution, all filaments save one were plucked and removed under an optical microscope with the help of a micromanipulator. The solution was then gradually replaced with isopropyl alcohol to reduce the surface tension before removing the finished device, as the surface tension of water is sure to break the filaments. More details on fabrication can be found in Ref. [37].

A total of three devices were produced, with thicknesses of d =530, 560, 900 nm. The devices were installed inside two channels of square cross-section 4 mm × 4 mm differing in length, fitted with NdFeB magnets to provide the driving field of 300 mT (short channel) and 410 mT (long channel) at room temperature, see Fig. 1. The standard magnetomotive scheme was used to drive the devices, with the relations of current I vs. force F, and voltage U vs. velocity v, given by [31]:

$$F = 0.523\, IBL_{\perp}, \quad U = 0.523\, vBL_{\perp}, \tag{4}$$

where $L_{\perp}$ is the length of the wire perpendicular to the direction of motion. This calibration satisfies the requirement that the dissipated powers expressed in terms of mechanical and electrical quantities match. Here B is the external magnetic field and the numerical prefactor describes the geometry of the resonant mode shape determined from Euler-Bernoulli beam theory for a doubly clamped thin beam. The effective mass in vacuum is then given by $m_{\text{eff}} = 0.396m$, where m is the mass of the suspended filament (obtained using its total length L, diameter D and density ρ_{NbTi}) [31]. The effective mass in helium will differ by the hydrodynamic added mass, leading to a small shift of the resonance frequency. For a cylinder in potential flow of helium, the hydrodynamic added mass is given by $m_{\text{hd}} = V\rho_{He}/2$, where V is the volume of the cylinder, representing a small correction due to the relative densities helium and NbTi.

The resonant frequencies of the devices necessarily depend on the tension in the filaments after cooldown. Without significant tension, they fall close to 1 kHz, but in one run with the 530 nm device, tension caused the fundamental resonance to shift as high as 30 kHz and forced the NEMS wire into string-like oscillations. This leads to a much higher quality factor and for a string-like resonance, the numerical prefactor in Eq. (4) becomes exactly 0.5 and the vacuum effective mass $m_{\text{eff}} = m/2$ [10].

The devices were driven by a bias current I created using a Rigol waveform generator and a 100 kΩ resistor. The Faraday voltage was amplified 50 times by an SR-560 voltage pre-amplifier with a 100 Hz - 10 kHz band pass filter and detected using an SR-830 lock-in. The external magnetic field was provided by permanent NdFeB magnets and due to the spin reorientation transition near 135 K, its value at low temperature is estimated as 78% of its value at room temperature [38]. The resulting magnetic field for the 560 nm device was thus 320(6) mT, while for the other two devices it was 234(4) mT.

3 Results and discussion

The resonance curves of the three devices in liquid helium are shown in Fig. 2. Despite very similar device dimensions, the 530 nm device exhibits a much higher resonance frequency and quality factor due to tension. However, on a subsequent cooldown this device was also tensionless, resonating close to 1.5 kHz, clearly showing the need for

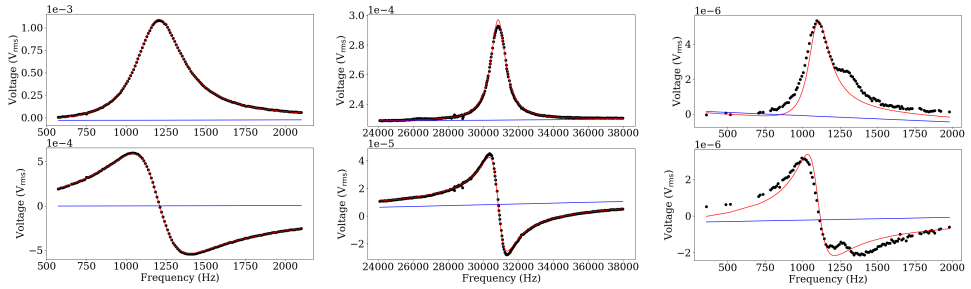

Fig. 2 Fundamental resonances of all three nanowires in liquid helium at 1.50 K: 560 nm (left), 530 nm (center) and 900 nm (right). The red curves represent Lorentzian fits and the straight blue lines are the backgrounds. The 530 nm device was the only one under tension when it cooled down and exhibits by far superior quality factors ($Q > 30$) compared to the other devices $Q \simeq 4$. The double-peak on the 900 nm device is likely caused by geometrical imperfections at the point of detachment of the single NbTi filament from the stronger Cu matrix, resulting in splitting of the two orthogonal vibrational modes.

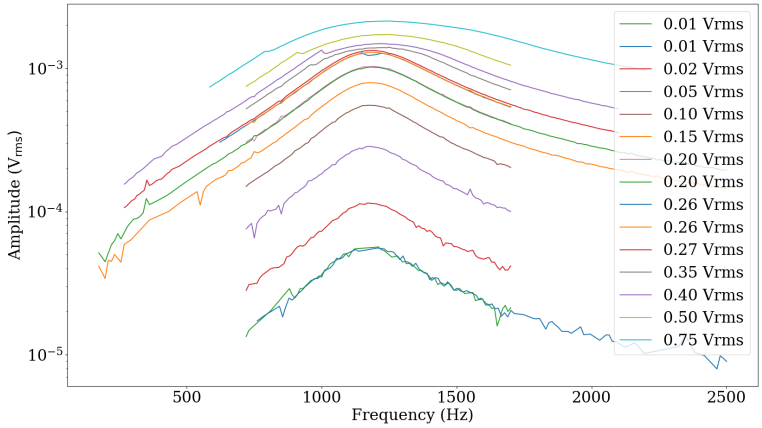

Fig. 3 Frequency sweeps taken with the 560 nm device at 1.50 K and varied drive levels between 0.01 V and 0.75 V. Symmetrical Lorentzian peaks observed at low drives become flattened and acquire asymmetric profiles as the drive increases.

precise control of the tension using a new production/mounting procedure that would guarantee reproducibility. We note that the low quality factors may be partly due to the relatively high applied magnetic fields.

The most sensitive 530 nm device was subsequently used to detect externally applied thermal counterflow, and the results will be discussed elsewhere. The double-peak structure of the 900 nm resonator precluded further experiments due to complications in the analysis. Therefore, we will focus exclusively on the 560 nm wire that was used to study the transition to turbulence in self-generated flow. We note that for this device $L_\perp = 2.0$ mm, while the total length was close to 3.0 mm.

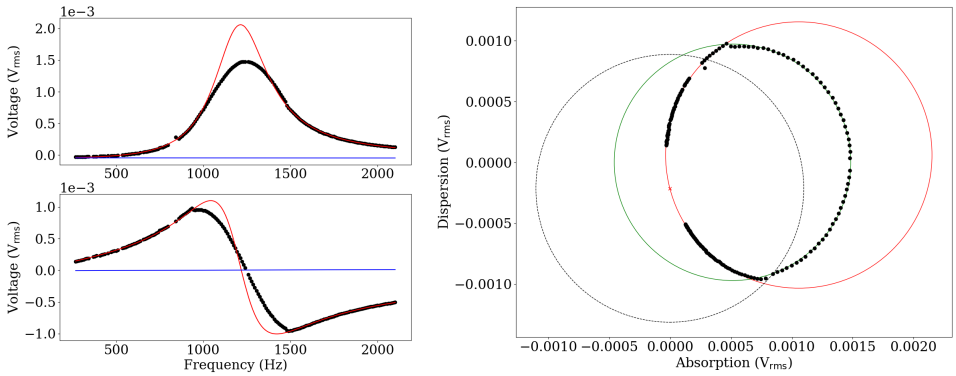

Fig. 4 Left: A resonant response exhibiting linear damping at low amplitudes (Lorentzian tails). The red curve is a fit to the tails of the curve defined as all points below a certain level. Right: The Nyquist plot of the same resonance. The Lorentzian tails correspond to the red circle, while the flattened top of the peak is described rather well by a shifted green circle of a lower diameter (amplitude). The black dashed circle is an estimate of the (lower) critical amplitude, see text.

A series of frequency sweeps and amplitude sweeps were recorded with this device at several temperatures between 1.43 K and 1.95 K at saturated vapour pressure. The frequency sweeps taken at 1.50 K are illustrated in Fig. 3 and show the same qualitative behaviour as numerous other works with resonators in superfluid helium. At low drives, a clean Lorentzian response is observed, which changes into a flattened-top peak at higher drives due to non-linear dissipation. An example of a non-linearly damped peak is shown in Fig. 4. The resonance curve can be rather clearly divided into Lorentzian tails (sub-critical, linear drag) and a central region with suppressed amplitude, or a higher and amplitude-dependent damping. It is somewhat surprising to see that the central part of the peak dominated by non-linear damping is quite precisely described by a circle in the Nyquist plot. This behaviour was present for both the 560 nm and the 530 nm devices and at a wide range of drive levels, but becomes less clear at the highest drives used. Being far from an experimental coincidence, the connection between the parameters of this circle and the dependence of the drag force on the oscillation velocity will be investigated further.

The amplitude sweeps revealed an expected form of force-velocity characteristics, with a linear regime at low drives, dominated by viscous drag, that transitions to a non-linear dependence above a certain critical velocity. The graph may be found in Fig. 5, together with the plot of a classical drag coefficient, $C_{\mathrm{D}} = 2F/(A\rho v^2)$, vs. velocity and the normal fluid drag coefficient, $C_{\mathrm{DN}} = 2F/(A\rho_n v^2)$, vs. the extended Donnelly number, Dn^*. Note the region of hysteresis present at all investigated temperatures. In previous works with larger devices, hysteresis was usually found only around or below 1 K [11, 19], but here persists at least up to 1.95 K, where $\rho_n \simeq \rho_s$. We are convinced that this is due to the size of the device and the number of remnant quantized vortices that it can interact with prior to generating new vortices upon triggering the turbulent instability.

This instability is characterized by a critical velocity consistent up to a factor of two with the value $v_{\mathrm{crit}} = \sqrt{8\kappa\omega}$ obtained from considerations of vortex dynamics in

oscillatory flow [39]. The extended Donnelly number describes well the viscous drag force (all data are within a 50% margin), but does not account for the instability, as there is no clear critical value of Dn*. This shows that the instability originates in the superfluid component.

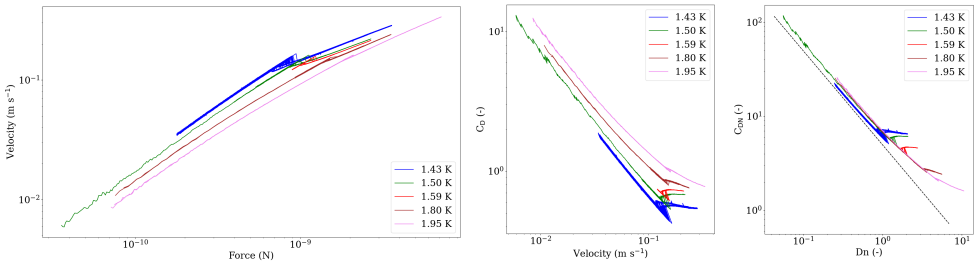

Fig. 5 Left: Force-velocity curves of the 560 nm wire at all investigated temperatures. Linear dependence is found at low drives up to a well-defined critical velocity $\approx$ 0.15 m/s. Center: Classically defined drag coefficient, C_D vs. velocity. Right: Normal fluid drag coefficient, C_{DN} vs. extended Donnelly number, Dn*. The black dashed line shows the analytical solution for an oscillating thin doubly clamped beam obtained from Eqs. (2) and (3). Hysteresis at the turbulent transition is clearly seen on all curves, but becoming systematically more pronounced as the temperature is decreased.

Upon close inspection, an interesting feature is visible close to the turbulent transition in the data taken at the lowest temperature reached, 1.43 K. A zoomed view of the 30 amplitude sweeps taken at 1.43 K is shown separately in Fig. 6 for clarity. A total of three metastable states exist close to the critical velocity, one in laminar flow, and two corresponding to turbulence.

A similar pattern has been observed more clearly in flow due to fourth sound resonances in nanomachined devices of a high aspect ratio [23]. In their work, the observed 2D flow multistability is analysed within a mathematical model using modal decomposition of the distributions of vortices in a 2D Onsager gas. While one may find it difficult to justify using a similar approach in 3D flow, we note that the laminar flow past an axially symmetric body (cylinder), in fact, closely resembles the 2D scenario and that the vorticity generated in its wake will also have a well-defined direction if insufficient turbulent mixing occurs close above the critical velocity. We may thus be dealing with the interplay of the two boundaries of the wake past the cylindrical wire. In classical steady flow past a cylinder, depending on the Reynolds number, the wake may either consist of two symmetric vortices (Re$\approx$ 20) or show vortices being shed in an anti-symmetric alternating fashion – the famous Kármán vortex street (Re$\approx$ 100), see, e.g., Ref. [40].

At the same time, it is fair to mention other possible mechanisms that may explain this observation. It is possible that the two branches correspond to two distinct situations: (i) with no vortex attached along the wire, and (ii) wire with a vortex attached length-wise, potentially closed as a loop through the Cu supports and base. These two situations would be topologically stable to small disturbances (explaining the lack of transitions between these two states) and could well result in different levels of energy

dissipation. At higher temperatures, such a trapped loop of quantized circulation may be de-stabilized by normal fluid flow via mutual friction.

On the other hand, we can quite reliably rule out the scenario in which turbulence is generated at two distinct places along the wire. The fact that the effect is present at 1.43 K and absent at 1.50 K and all higher temperatures would hardly be explained with a purely geometry-dependent criterion.

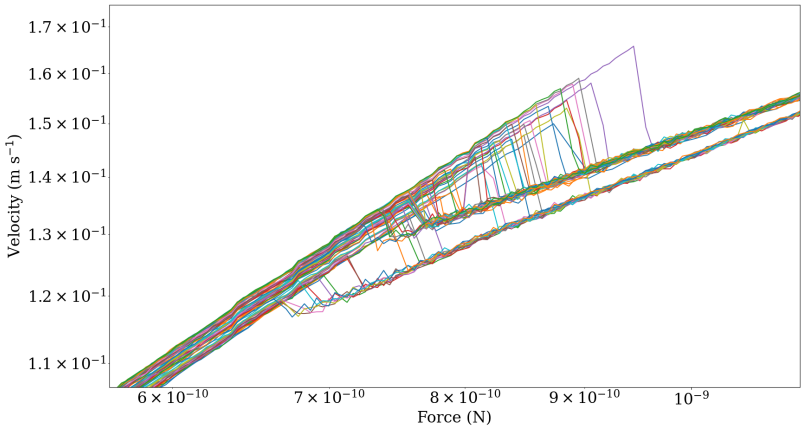

Fig. 6 A detailed view of the turbulent transition measured at 1.43 K. Note that two distinct branches exist in turbulent flow, alongside the metastable laminar flow. This multistability is observed with the 560 nm device only at this lowest temperature reached. Transitions between laminar flow and one of the turbulent states are relatively common, while jumps between the two turbulent states have not been documented in our data. As shown in Fig. 5, the two branches eventually approach and at higher velocities appear to coincide within our resolution.

4 Conclusion

Several NbTi nanowires of macroscopic length were characterised in superfluid helium and it was found that their properties are profoundly influenced by their tension, implying the need to control the tension in all future work. Viscous dissipation experienced by these devices is described with acceptable accuracy by known scaling laws adjusted to extend their validity beyond the high frequency (high Stokes number) limit.

The transition to turbulent drag in oscillatory flow was investigated with one of the devices, with strong hysteresis found at all investigated temperatures. The range of velocities corresponding to the hysteretic region increases at lower temperatures, in agreement with previous works [11, 19], where hysteresis was more often found only at mK temperatures.

The origin of the turbulent instability in the superfluid component was confirmed, with a critical velocity of 0.15 m/s, within a factor of two from the velocity estimated

in Ref. [39]. Notably, multistability of the flow was observed at the lowest temperature of 1.43 K, with three separate metastable states. Transitions from the single laminar state to either of the two turbulent states were observed, with no direct evidence for transitions between the two turbulent states, suggesting their robustness to small disturbances such as those in a weakly turbulent flow. At high velocities, the two turbulent states became indistinguishable within our resolution. With our limited data, we can at this point neither confirm nor disprove the underlying mechanism behind a similar multistable flow observed in a microfluidic Helmholtz resonator subject to 2D oscillatory flow realized by fourth sound.

Future work will focus on the ability of nanowires to detect external flow, on the preparation of wires under reproducible tension, and we will aim to investigate the interaction of these devices with individual quantized vortices, both above 1 K and at mK temperatures.

Acknowledgements. The authors appreciate fruitful discussions with S. Autti, S. Kafanov and V. B. Eltsov and the assistance of B. Vejr with the manufacturing of channel components. This research was supported by the Czech Science Foundation, Grant No. 24-12253S. DEZ acknowledges support by UKRI (project EP/X004597/1).

References

[1] Avila, K., Moxey, D., Lozar, A., Avila, M., Barkley, D., Hof, B.: The Onset of Turbulence in Pipe Flow. Science **333**(6039), 192–196 (2011) https://doi.org/10.1126/science.1203223

[2] Mullin, T.: Experimental Studies of Transition to Turbulence in a Pipe. In: Davis, SH and Moin, P (ed.) ANNUAL REVIEW OF FLUID MECHANICS, VOL 43. Annual Review of Fluid Mechanics, vol. 43, pp. 1–24 (2011). https://doi.org/10.1146/annurev-fluid-122109-160652

[3] Honji, H.: Streaked Flow Around an Oscillating Circular-Cylinder. J. Fluid Mech. **107**, 509–520 (1981) https://doi.org/10.1017/S0022112081001894

[4] Hall, P.: On the Stability of the Unsteady Boundary-Layer on a Cylinder Oscillating Transversely in a Viscous Fluid. J. Fluid Mech. **146**, 347–367 (1984) https://doi.org/10.1017/S0022112084001907

[5] Sarpkaya, T.: Force on a Circular-Cylinder in Viscous Oscillatory Flow at Low Keulegan-Carpenter Numbers. J. Fluid Mech. **165**, 61–71 (1986) https://doi.org/10.1017/S0022112086002999

[6] Obasaju, E.D., Bearman, P.W., Graham, J.M.R.: A Study of Forces, Circulation and Vortex Patterns Around a Circular-Cylinder in Oscillating Flow. J. Fluid Mech. **196**, 467 (1988) https://doi.org/10.1017/S0022112088002782

[7] Tatsuno, M., Bearman, P.W.: A Visual Study of the Flow Around an Oscillating Circular-Cylinder at Low Keulegan-Carpenter Numbers and Low

Stokes Numbers. J. Fluid Mech. **211**, 157–182 (1990) https://doi.org/10.1017/S0022112090001537

[8] Nichol, H.A., Skrbek, L., Hendry, P.C., McClintock, P.V.E.: Flow of He II due to an Oscillating Grid in the Low-Temperature Limit. Phys. Rev. Lett. **92**(24) (2004) https://doi.org/10.1103/PhysRevLett.92.244501

[9] Charalambous, D., Skrbek, L., Hendry, P.C., McClintock, P.V.E., Vinen, W.F.: Experimental investigation of the dynamics of a vibrating grid in superfluid He-4 over a range of temperatures and pressures. Phys. Rev. E **74**(3, Part 2) (2006) https://doi.org/10.1103/PhysRevE.74.036307

[10] Morishita, M., Kuroda, T., Sawada, A., Satoh, T.: Mean Free Path Effects in Superfluid 4He. J. Low Temp. Phys. **76**(5-6), 387 (1989) https://doi.org/10.1007/BF00681736

[11] Goto, R., Fujiyama, S., Yano, H., Nago, Y., Hashimoto, N., Obara, K., Ishikawa, O., Tsubota, M., Hata, T.: Turbulence in boundary flow of superfluid He-4 triggered by free vortex rings. Phys. Rev. Lett. **100**(4) (2008) https://doi.org/10.1103/PhysRevLett.100.045301

[12] Bradley, D.I., Fisher, S.N., Guenault, A.M., Haley, R.P., Tsepelin, V., Pickett, G.R., Zaki, K.L.: The Transition to Turbulent Drag for a Cylinder Oscillating in Superfluid He-4: A Comparison of Quantum and Classical Behavior. J. Low Temp. Phys. **154**(3-4), 97–116 (2009) https://doi.org/10.1007/s10909-008-9858-7

[13] Collin, E., Kofler, J., Heron, J.S., Bourgeois, O., Bunkov, Y.M., Godfrin, H.: Novel "Vibrating Wire Like" NEMS and MEMS Structures for Low Temperature Physics. J. Low Temp. Phys. **158**(3-4), 678–684 (2010) https://doi.org/10.1007/s10909-009-9960-5

[14] Jager, J., Schuderer, B., Schoepe, W.: Turbulent and Laminar Drag of Superfluid Helium on an Oscillating Microsphere. Phys. Rev. Lett. **74**(4), 566–569 (1995) https://doi.org/10.1103/PhysRevLett.74.566

[15] Niemetz, M., Schoepe, W.: Stability of Laminar and turbulent flow of superfluid He-4 at mK temperatures around an oscillating microsphere. J. Low Temp. Phys. **135**(5-6), 447–469 (2004) https://doi.org/10.1023/B:JOLT.0000029507.98543.1d

[16] Donnelly, R.J., Hollis Hallett, A.C.: Periodic Boundary Layer Experiments in Liquid Helium. Annals of Physics **3**(3), 320–345 (1958) https://doi.org/10.1016/0003-4916(58)90023-X

[17] Blažková, M., Schmoranzer, D., Skrbek, L.: Transition from laminar to turbulent drag in flow due to a vibrating quartz fork. Phys. Rev. E **75**(2, Part 2) (2007) https://doi.org/10.1103/PhysRevE.75.025302

[18] Blažková, M., Schmoranzer, D., Skrbek, L., Vinen, W.F.: Generation of turbulence by vibrating forks and other structures in superfluid He-4. Phys. Rev. B **79**(5) (2009) https://doi.org/10.1103/PhysRevB.79.054522

[19] Bradley, D.I., Fear, M.J., Fisher, S.N., Guenault, A.M., Haley, R.P., Lawson, C.R., McClintock, P.V.E., Pickett, G.R., Schanen, R., Tsepelin, V., Wheatland, L.A.: Transition to Turbulence for a Quartz Tuning Fork in Superfluid He-4. J. Low Temp. Phys. **156**(3-6), 116–131 (2009) https://doi.org/10.1007/s10909-009-9901-3

[20] Garg, D., Efimov, V.B., Giltrow, M., McClintock, P.V.E., Skrbek, L., Vinen, W.F.: Behavior of quartz forks oscillating in isotopically pure He-4 in the T = 0 limit. Phys. Rev. B **85**(14) (2012) https://doi.org/10.1103/PhysRevB.85.144518

[21] Rojas, X., Davis, J.P.: Superfluid nanomechanical resonator for quantum nanofluidics. Phys. Rev. B **91**(2) (2015) https://doi.org/10.1103/PhysRevB.91.024503

[22] Varga, E., Vadakkumbatt, V., Shook, A.J., Kim, P.H., Davis, J.P.: Observation of bistable turbulence in quasi-two-dimensional superflow. Phys. Rev. Lett. **125**, 025301 (2020) https://doi.org/10.1103/PhysRevLett.125.025301

[23] Novotný, F., Talíř, M., Midlik, v., Varga, E.: Critical behavior and multistability in quasi-two-dimensional turbulence. Phys. Rev. Fluids **10**, 054605 (2025) https://doi.org/10.1103/PhysRevFluids.10.054605

[24] Guenault, A.M., Guthrie, A., Haley, R.P., Kafanov, S., Pashkin, Y.A., Pickett, G.R., Poole, M., Schanen, R., Tsepelin, V., Zmeev, D.E., Collin, E., Maillet, O., Gazizulin, R.: Probing superfluid He-4 with high-frequency nanomechanical resonators down to millikelvin temperatures. PHYSICAL REVIEW B **100**(2) (2019) https://doi.org/10.1103/PhysRevB.100.020506

[25] Kamppinen, T., Eltsov, V.B.: Nanomechanical Resonators for Cryogenic Research. JOURNAL OF LOW TEMPERATURE PHYSICS **196**(1-2), 283–292 (2019) https://doi.org/10.1007/s10909-018-02124-z . 23rd International Symposium on Quantum Fluids and Solids (QFS), Univ Tokyo, Ito Int Res Ctr, Tokyo, JAPAN, JUL 25-31, 2018

[26] Kamppinen, T., Mäkinen, J.T., Eltsov, V.B.: Superfluid ^{4}He as a rigorous test bench for different damping models in nanoelectromechanical resonators. Phys. Rev. B **107**, 014502 (2023) https://doi.org/10.1103/PhysRevB.107.014502

[27] Tisza, L.: Transport phenomena in helium II. Nature **141**, 913 (1938)

[28] Landau, L.D.: On the Theory of Superfluidity. Physical Review **75**(5), 884–885 (1949)

[29] Feynman, R.P.: Helium-II in Rotational Flow. Science **121**(3148), 622 (1955)

[30] Vinen, W.F.: Detection of Single Quanta of Circulation in Liquid Helium-II. Proc. Royal Soc. London Series A-Math. Phys. Sciences **260**(130), 218 (1961)

[31] Schmoranzer, D., Jackson, M.J., Midlik, S., Skyba, M., Bahyl, J., Skokankova, T., Tsepelin, V., Skrbek, L.: Dynamical similarity and instabilities in high-Stokes-number oscillatory flows of superfluid helium. PHYSICAL REVIEW B **99**(5) (2019) https://doi.org/10.1103/PhysRevB.99.054511

[32] Midlik, i.c.v., Schmoranzer, D., Skrbek, L.: Transition to quantum turbulence in oscillatory thermal counterflow of ^{4}He. Phys. Rev. B **103**, 134516 (2021) https://doi.org/10.1103/PhysRevB.103.134516

[33] Skrbek, L., Schmoranzer, D., Midlik, Sreenivasan, K.R.: Phenomenology of quantum turbulence in superfluid helium. Proceedings of the National Academy of Sciences **118**(16), 2018406118 (2021) https://doi.org/10.1073/pnas.2018406118 https://www.pnas.org/doi/pdf/10.1073/pnas.2018406118

[34] Stokes, G.G.: On the Effect of the Internal Friction of Fluids on the Motion of Pendulums. Cambridge Library Collection - Mathematics, pp. 1–10. Cambridge University Press, Cambridge, UK (2009)

[35] Drazin, P.G., Riley, N.: London Mathematical Society Lecture Note Series: The Navier-stokes Equations: A Classification of Flows and Exact Solutions Series Number 334. Cambridge University Press, Cambridge, England (2009)

[36] Wang, C.-Y.: On high-frequency oscillatory viscous flows. Journal of Fluid Mechanics **32**(1), 55–68 (1968) https://doi.org/10.1017/S0022112068000583

[37] Autti, S., Casey, A., Connelly, M., Darvishi, N., Franchini, P., Gorman, J., Haley, R.P., Heikkinen, P.J., Kemp, A., Leason, E., March-Russell, J., Monroe, J., Noble, T., Pickett, G.R., Prance, J.R., Rojas, X., Salmon, T., Saunders, J., Slater, J., Smith, R., Thompson, M.D., West, S.M., Whitehead, L., Zavjalov, V.V., Zhang, K., Zmeev, D.E.: Long nanomechanical resonators with circular cross-section (2023). https://doi.org/10.48550/arXiv.2311.02452 . https://arxiv.org/abs/2311.02452

[38] Hu, J., Kou, X.C., Kronmüller, H.: The low-temperature dependence of coercivity in ndfeb magnets. physica status solidi (b) **188**(2), 807–811 (1995) https://doi.org/10.1002/pssb.2221880224 https://onlinelibrary.wiley.com/doi/pdf/10.1002/pssb.2221880224

[39] Hanninen, R., Schoepe, W.: Universal Onset of Quantum Turbulence in Oscillating Flows and Crossover to Steady Flows. J. Low Temp. Phys. **158**(3-4), 410–414 (2010) https://doi.org/10.1007/s10909-009-9972-1

[40] Van Dyke, M.: An Album of Fluid Motion. Parabolic Press, Stanford, CA (1982)